

Pulsed neutron source measurements in the subcritical ADS experiment YALINA-Booster

Carl-Magnus Persson^{a,*}, Andrei Fokau^{a,b}, Ivan Serafimovich^b, Victor Bournos^b, Yurii Fokov^b, Christina Routkovskaia^b, Hanna Kiyavitskaya^b, Waclaw Gudowski^a

^a Royal Institute of Technology, AlbaNova University Centre, Department of Reactor Physics, SE-106 91, Stockholm, Sweden

^b Joint Institute for Power and Nuclear Research, National Academy of Sciences of Belarus, Minsk, Belarus

ARTICLE INFO

Article history:

Received 25 July 2008

Accepted 29 July 2008

Available online 21 September 2008

ABSTRACT

A subcritical zero-power source-driven coupled core, the YALINA-Booster, has been constructed for experimental investigations of neutron kinetics of source-driven systems. In this study, the reactivity of two subcritical configurations has been determined by the area ratio method. The prompt neutron decay constants have been evaluated through slope fitting of the prompt neutron decay as well as through the pulsed Rossi- α method. It is shown that the slope fitting method and the pulsed Rossi- α method give stable results whereas the area ratio method results show spatial dependence. The reasons for the spatial spread are addressed.

© 2008 Elsevier Ltd. All rights reserved.

1. Introduction

Accelerator-driven systems (ADS) may play an important role in future nuclear fuel cycles to reduce the long-term radiotoxicity and volume of spent nuclear fuel (OECD/NEA, 2002). In order to guarantee safe operation of reactor systems based on fuels containing high fractions of plutonium and minor actinides, they must operate in subcritical mode driven by an external neutron source. The subcriticality monitoring of such systems is a necessity, but it is still an open question how it will be performed (Mellier et al., 2005). A reactivity monitoring system will need to be calibrated and for that purpose, reactivity determination methods are required. In order to make a good calibration, information about the performance of the reactivity determination methods, in terms of accuracy and reliability, is of utmost importance. Recent studies (Rubbia et al., 2003; Soule et al., 2004; Persson et al., 2005) have been devoted to determining reactivity at low power in thermal or fast systems. Since this study is based on a heterogeneous coupled fast-thermal core, the kinetic response and characteristics will be different from previous studies. Moreover, YALINA-Booster is a subcritical assembly without access to a critical reference configuration. Without a critical reference level, where the physics is well known, there is no possibility of determining the reactivity of subcritical configurations by conventional methods based on, for instance, movements of calibrated control rods. On the other hand, this is the situation that will be faced when a full-scale facility is commissioned in future. Reactivity determination methods based on a localized detec-

tor will give results carrying spatial dependence. Such effects are also discussed in this paper.

2. Reactivity determination with a pulsed neutron source

2.1. Slope fitting

The idea of using the prompt neutron decay constant, defined as

$$\alpha = \frac{1}{n} \frac{dn}{dt} = \frac{\rho - \beta_{\text{eff}}}{A}, \quad (1)$$

where n is the neutron density, for subcriticality determination purposes, was proposed by Simmons and King (1958). As can be found from Eq. (1), a drawback of this method is that for the determination of the reactivity from a measurement of the prompt neutron decay constant, one must know the effective delayed neutron fraction, β_{eff} , and the neutron reproduction time (Lewis, 2006), A .

The prompt neutron decay constant can be determined by fitting an exponential function to the detector response of a neutron pulse insertion. However, only one pulse is not enough to find the slope with sufficient accuracy, hence raising the need for a pulsed neutron source and to acquire the pulses in a histogram. Therefore, this method of finding α for reactivity determination is here referred to as the slope fitting method, but various names have been used in other papers.

2.2. Area ratio

Sjöstrand (1956) showed that the reactivity in the unit of dollar can be obtained from a pulsed neutron source (PNS) histogram according to

* Corresponding author. Tel.: +46 8 5537 8204.

E-mail address: calle@neutron.kth.se (C.-M. Persson).

$$\rho_s = \frac{\rho}{\beta_{\text{eff}}} = -\frac{A_p}{A_d}. \quad (2)$$

The prompt neutron area, A_p , and the delayed neutron area, A_d , are depicted in Fig. 1. If there is a non-negligible contribution from an inherent source, e.g. spontaneous fissions, it must be subtracted as well. An advantage of this method is that it does not require any calibration at delayed critical and that the measured quantities are integrals, thus reducing the statistical uncertainty.

This method, as well as the slope fitting method, is based on the assumption that the point-kinetics approximation is valid. If so, an estimate of the ratio ρ/β_{eff} can be found by rewriting Eq. (1) and including experimental data from the area method as well as the slope fitting method

$$\frac{\rho}{\beta_{\text{eff}}} = \frac{1}{\alpha} \left(\frac{\rho}{\beta_{\text{eff}}} - 1 \right). \quad (3)$$

2.3. Rossi- α with pulsed source

The pulsed Rossi- α formula has been derived based on the backward master equation technique by Kitamura et al. (2006). In its most general form, the pulsed Rossi- α formula can be expressed as

$$p(t) dt = A_1 e^{\alpha t} dt + A_2 dt + A_3 \sum_{n=1}^{\infty} (a_n^2 + b_n^2) \cos(\omega_n t) dt. \quad (4)$$

The constants A_i , $i = 1, 2, 3$, are given in the paper of Kitamura et al. (2006). Depending on the shape and frequency of the neutron source pulse, the parameters A_3 , a_n , b_n and ω_n will be different (based on a Fourier series of the neutron source time characteristics). However, the main structure of Eq. (4) is maintained independently of the specific source characteristics. The first two terms have the same meaning as in the traditional Rossi- α formula: one exponentially decreasing correlated term and a constant uncorrelated term. The third oscillating term is uncorrelated and non-decaying, caused by the pulsed source.

3. The YALINA-Booster

The YALINA-Booster is a subcritical fast-thermal core coupled to a neutron generator (NG-12-1). The main parts of the neutron generator are the deuteron ion accelerator and a Ti-T or Ti-D neutron production target, with a diameter of 45 mm, located in the centre of the core. The neutron energy is around 14 MeV for the DT- and

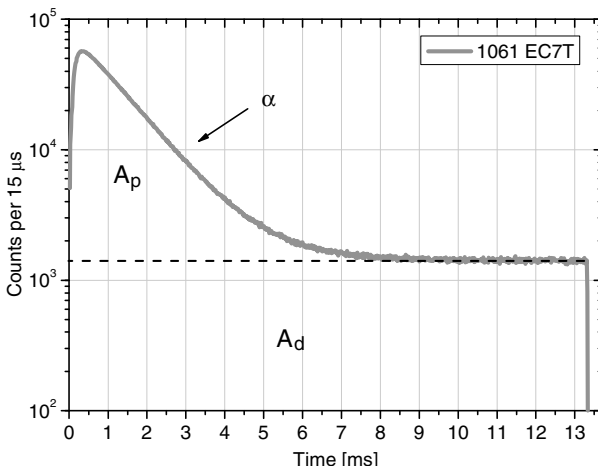


Fig. 1. Prompt and delayed neutron areas used in the area method, as well as the exponential decay of prompt neutrons for the 1061-configuration in the experimental channel EC7T (time bin = 15 μ s).

2.5 MeV for the DD-reaction. The neutron generator can be operated in both continuous and pulse mode and provides the possibility to generate pulses with frequencies from 1 Hz to 7 kHz with pulse duration of 2–130 μ s. The maximum beam current in continuous mode is 2 mA with a beam diameter about 20 mm giving a maximum neutron yield of approximately 2×10^{11} neutrons per second for the Ti-T target and 2×10^9 neutrons per second for the Ti-D target.

The core, depicted in Fig. 2, consists of a central lead zone, a polyethylene zone, a radial graphite reflector and a front and back biological shielding of borated polyethylene. The loading is 132 fuel pins containing metallic uranium of 90% enrichment, 563 fuel pins containing uranium dioxide of 36% enrichment and a maximum of 1141 EK-10 fuel pins containing uranium dioxide of 10% enrichment. No active cooling of the core is needed.

The fast-spectrum lead zone and the thermal-spectrum polyethylene zone are separated by a so called thermal neutron filter, or valve zone, consisting of one layer of 108 pins with metallic natural uranium and one layer of 116 pins with boron carbide (B_4C) which are located in the outermost two rows of the fast zone. Thermal neutrons diffusing from the thermal zone to the fast zone will either be absorbed by the boron or by the natural uranium, or transformed into fast neutrons through fission in the natural uranium. In this way, a coupling of mainly fast neutrons between the two zones is maintained.

There are seven axial experimental channels (EC1B–EC4B and EC5T–EC7T) in the core and two axial (EC8R and EC9R) and one radial experimental channel (EC10R) in the reflector. Moreover, there is one neutron flux monitoring channel in each corner of the core. Three B_4C -control rods, with a total reactivity worth of approximately $-0.5\$$, can be inserted in the thermal zone. A more detailed description is available in the IAEA YALINA-Booster benchmark description (Kiyavitskaya et al., 2007).

In these measurements two configurations were studied. These configurations have a fully loaded fast zone, as described above, and 1132 and 1061 fuel pins of 10% enrichment in the thermal zone respectively. The loading of these fuel pins was made based on cylindrical symmetry, whereas the fuel pins of the booster region are loaded in square geometry. In all measurements the three control rods were completely extracted.

4. Methodology

All measurements were performed using a Ti-D target for neutron production and a 3He -detector, sensitive mainly to thermal neutrons, for neutron detection. Data were acquired using a counter/timer card that stores the arrival time of each detection event from the 3He -detector and the trigger signal from the neutron generator. The accuracy of the time stamping is 12.5 ns and the total dead time of the electronic chain is 3.3 μ s. Having access to all events from the experiment, any data analysis can be performed off-line, after the experiment has been performed. In parallel, data were recorded with a multi-scaler to ensure the reliability of the two data acquisition systems. The advantage of using a counter/timer is that except for the PNS histogram construction capability also noise analysis can be performed in a convenient way.

5. Experimental results

5.1. Slope fitting

PNS measurements were performed with the detector subsequently located in the experimental channels EC5T–EC9R. The pulse response histograms are shown in Figs. 3 and 4 for the two

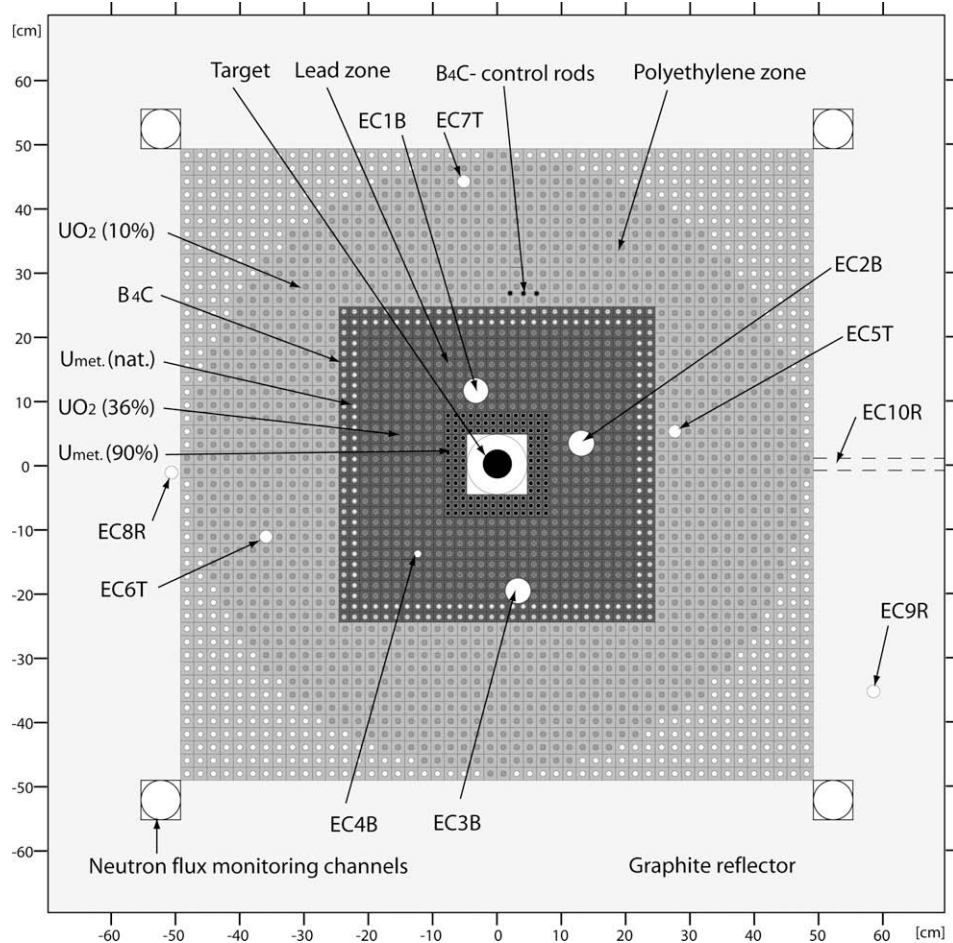


Fig. 2. Schematic cross-sectional view of YALINA-Booster (the 1132-configuration).

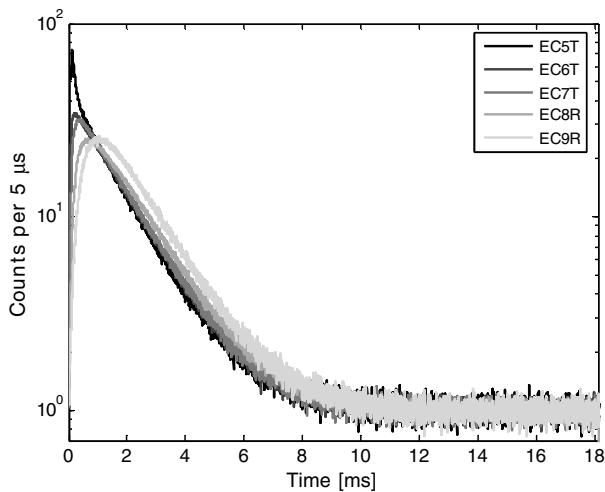


Fig. 3. PNS histograms, normalised to the delayed neutron background, for the 1132-configuration.

configurations respectively. In both figures the time scale is kept the same for better illustration of the difference in prompt neutron decay. In contrast to the previous YALINA experiment (Persson et al., 2005), a clear fundamental mode decay was visible in all experimental channels, thus simplifying the analysis. The function minimisation tool Minuit (James and Winkler, 2004) was used to fit a function of the type

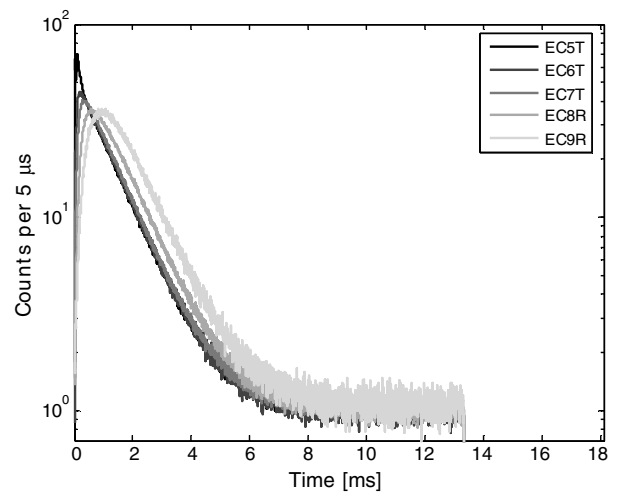


Fig. 4. PNS histograms, normalised to the delayed neutron background, for the 1061-configuration.

$$f(t) = A_1 e^{\alpha t} + A_2 \quad (5)$$

to the obtained histograms. In this way, by simultaneous fitting of all parameters, the nonlinear relation between the parameters is accounted for correctly. This procedure gives both the prompt neutron decay constant, α , and the constant level, A_2 , which is used for the area method when separating the prompt and the delayed

neutron areas. The delayed background is in fact also decaying exponentially with a rate comparable to the fastest delayed neutron precursor group ($\sim 3 \text{ s}^{-1}$). However, in this time interval, shorter than 20 ms, this decay was not observed. In the fitting procedure, the first part of the signal was not considered and a sensitivity analysis of the fitting start-point was performed. For all cases, the reduced χ^2 deviated less than 1% from unity. As can be seen in Table 1 and Fig. 5, the resulting prompt neutron decay constants can be achieved with high accuracy and small spatial spread (<2%).

5.2. Area ratio

From the fitting of Eq. (5) to the histograms the constant level of delayed neutrons, A_d , was obtained. Knowing the constant level, the reactivity in dollars was obtained after calculating the prompt and delayed neutron areas (Table 1). First, the background counts coming from the inherent source should be subtracted. However, in these measurements the inherent source was completely negligible. The obtained reactivity as a function of distance from the booster zone follows the same pattern in both configurations as can be seen in Fig. 6, thus indicating a systematic spatial spread. The reason for this spread will here be further discussed.

Since the reactivity is calculated from the prompt and delayed neutron areas, their individual spatial dependence is here investigated. First, the prompt and delayed area profiles, f_p and f_d , are defined as the ratio of the area in each point i divided by the average area

$$f_{x,i} = \frac{A_{x,i}}{\bar{A}_x}. \quad (6)$$

The variable x is either p or d for prompt and delayed area, respectively, and i represents the detector positions EC5T–EC9R. In the same manner, the *reactivity profile* is defined

$$f_{\rho,i} = \frac{\rho_{\$,i}}{\bar{\rho}_{\$}}. \quad (7)$$

If there is no spatial spread in the measured values of the reactivity, meaning that

$$f_{\rho,i} = 1 \quad \forall i, \quad (8)$$

then one of the following conditions must be fulfilled:

1. The prompt and delayed areas have *no* spatial spread

$$f_{p,i} = f_{d,i} = 1 \quad \forall i. \quad (9)$$

Table 1
Results from PNS measurements

Configuration	EC	$\alpha (\text{s}^{-1})$	$\rho/\beta_{\text{eff}} (\$)$	$A/\beta_{\text{eff}} (\text{ms})$
1132	EC5T	-654.1 ± 1.6	-3.60 ± 0.03	7.04 ± 0.04
	EC6T	-662.6 ± 1.8	-3.36 ± 0.02	6.58 ± 0.04
	EC7T	-649.4 ± 1.4	-3.37 ± 0.02	6.73 ± 0.03
	EC8R	-648.7 ± 2.0	-3.61 ± 0.02	7.11 ± 0.03
	EC9R	-644.0 ± 3.3	-3.92 ± 0.03	7.65 ± 0.05
Weighted mean value		-652.7	-3.54	6.96
Spread		7.1 (1.1%)	0.23 (6.5%)	0.42 (6.0%)
1061	EC5T	-875.0 ± 1.9	-5.09 ± 0.03	6.96 ± 0.03
	EC6T	-892.1 ± 2.7	-4.71 ± 0.03	6.40 ± 0.03
	EC7T	-866.7 ± 2.2	-4.75 ± 0.03	6.64 ± 0.03
	EC8R	-863.4 ± 3.2	-5.07 ± 0.03	7.03 ± 0.03
	EC9R	-860.1 ± 3.6	-5.33 ± 0.03	7.36 ± 0.04
Weighted mean value		-872.7	-4.95	6.82
Spread		12.9 (1.5%)	0.26 (5.3%)	0.38 (5.5%)

A/β_{eff} is calculated from the experimental values of α and ρ/β_{eff} relying on Eq. (3). The spread is evaluated with respect to the weighted mean value.

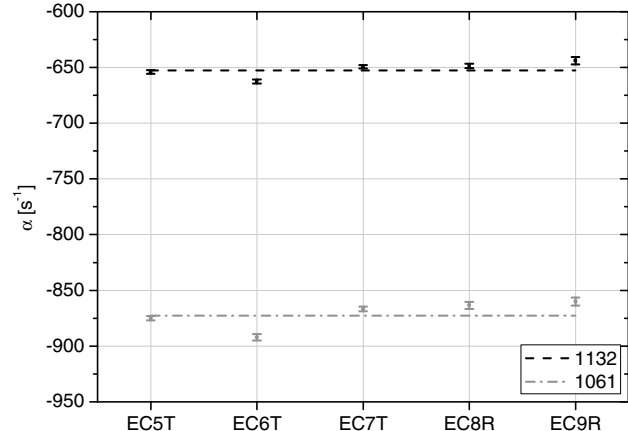


Fig. 5. Prompt neutron decay constants from the slope fitting method for different detector positions. The weighted mean values are indicated as straight lines.

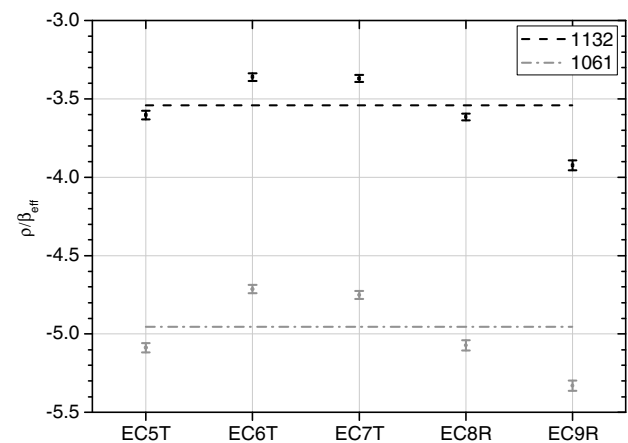


Fig. 6. Reactivity (in \$) from the area method for different detector positions. The weighted mean values are indicated as straight lines.

That would represent a trivial point kinetic case when the neutron flux is the same in the entire core.

2. The prompt and delayed areas have *the same* spatial spread

$$f_{p,i} = f_{d,i} \quad \forall i. \quad (10)$$

The second case may hold in a homogeneous core where the prompt and delayed neutron flux distributions are the same, and if the detector is located far from the source and the core boundaries. However, in a heterogeneous core, such as YALINA-Booster, this is not necessarily the case. Assume that the prompt and delayed area profiles have different shape and that there is a factor, γ , describing the non-similarity

$$f_{p,i} = \gamma_i f_{d,i}. \quad (11)$$

Then, the reactivity profile becomes

$$f_{\rho,i} = \frac{A_{p,i}}{A_{d,i}} = \frac{\gamma_i \bar{A}_p}{\bar{\gamma}_i \bar{A}_d} = \frac{\gamma_i \bar{A}_p}{\bar{\gamma} \bar{A}_d}, \quad (12)$$

where

$$\bar{\gamma} = \frac{\bar{A}_d}{\bar{A}_p} \bar{\rho}. \quad (13)$$

As a consequence, if γ is less than unity in one location, then γ must be larger than unity in another location to keep the average value of

the reactivity profile at unity and thus giving rise to a non-trivial spatial profile. As an illustration the profiles discussed above are depicted in Fig. 7 for the 1132-configuration.

There are two basic reasons why the measured reactivity differs from point to point; either the prompt area has changed relatively the delayed area or vice versa. The prompt area disturbance is usually ascribed higher harmonics during the first part of the pulse. In the detector signals from the experimental channel EC5T a very fast decay can be found during the first millisecond. This comes from non-fundamental mode neutrons escaping the booster zone. This is reflected in the area profiles depicted in Fig. 7 where there is a relative increase in prompt area for EC5T as compared to the delayed area.

It has been proposed (Bell and Glasstone, 1970) to decrease the spatial spread by simply ignoring the transient part of the PNS histogram by extrapolating the fundamental mode decay back to time zero (Gozani, 1962). In this way, the higher harmonics appearing just after the source pulse insertion are not taken into account. Results from this method, here referred to as the *extrapolated area ratio method*, are shown together with the traditional area ratio method for the 1132-configuration in Fig. 8. As can be seen, the extrapolated area ratio method gives very different results in the YALINA-Booster, especially in the reflector region where the reactivity is strongly underestimated. This behaviour can be understood simply by inspection of the PNS histograms in Figs. 3 and 4. If the fundamental slope in the reflector channels is extrapolated backwards the prompt area will be increased to a large extent while the delayed area remains constant. The effect is larger for experimental channels far from the source since the histogram maximum appears later in time. This effect should be even more pronounced for deeper subcriticalities since the faster prompt neutron decay will cause a larger constant in front of the exponential (A_1). The method might work better in cases where the detector is located closer to the source and the higher harmonics have higher amplitude.

The second reason why getting a spatial spread is related to the delayed area. The detector position EC5T is located close to the valve zone between the fast and thermal zones. In the valve zone there is a pin layer of boron carbide and ^{238}U that absorbs mainly thermal neutrons. Since the delayed neutrons in general have softer spectrum than the fission neutrons, as shown in Fig. 9, they tend to get absorbed to a larger extent in the boron. This effect acts in the same direction as the effect from the higher harmonics, thus making it hard to quantify. From Fig. 7 it is also possible to see that the delayed neutron profile decreases slightly faster than the prompt neutron profile when reaching further out in the reflector

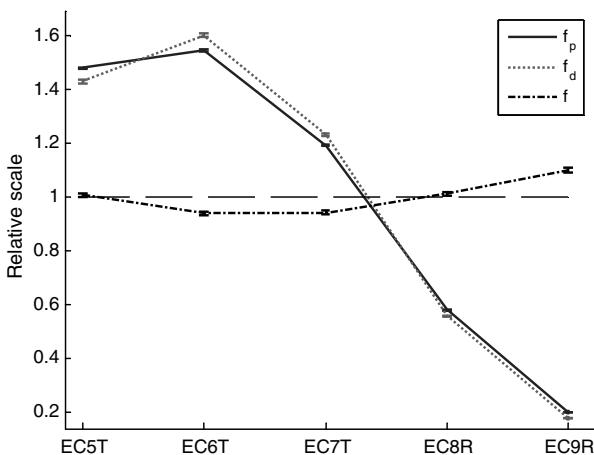


Fig. 7. Spatial profiles for the prompt and delayed areas as well as the reactivity for the 1132-configuration.

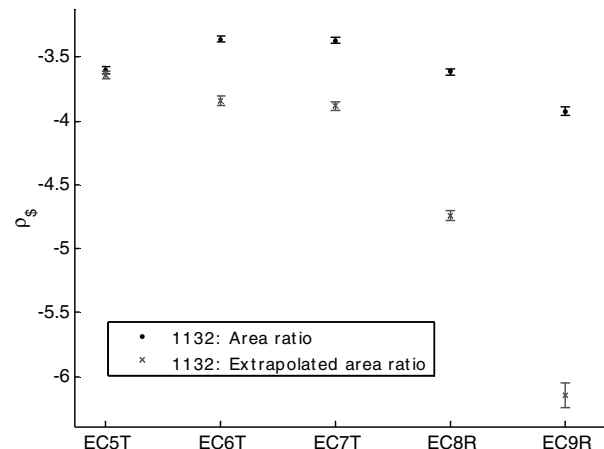


Fig. 8. Reactivity obtained from the traditional area ratio method and the extrapolated area ratio method.

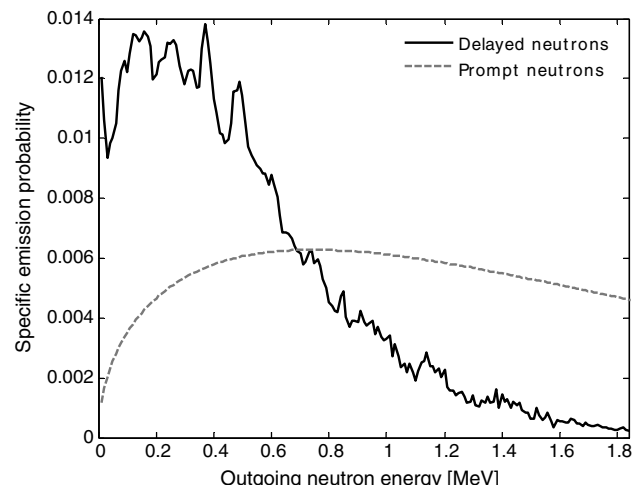


Fig. 9. Spectrum of delayed and prompt neutrons (from ENDF/B-VII).

region. This effect can also be ascribed the different energy distributions of prompt and delayed neutrons. All neutrons are born in the core region and some of them are diffusing out from the core to the reflector. Since the prompt neutrons in general have higher energy than the delayed neutrons, they reach with a larger probability further out in the reflector before getting absorbed or back-scattered. This effect leads consequently to an underestimation of the effective multiplication factor when evaluating signals from the reflector.

In the further analysis the weighted mean values of the obtained parameters from the slope fitting method and the area ratio method will be used as reference values. Since the spread in all cases is much larger than the statistical error in each point, the spread will be used as the uncertainty of the weighted mean value. A consequence of the systematic spatial spread is that the reactivity difference, as measured in each point, can be achieved with a low spatial spread: $\Delta\rho/\beta_{\text{eff}} = 1.41 \pm 0.05 \$$.

In Table 1, the ratio A/β_{eff} is shown, calculated from Eq. (3). These values are used later to estimate the neutron reproduction time.

5.3. Rossi- α with pulsed source

For large t , the correlated term of Eq. (4) is negligible. By considering a period of the oscillation term at large t and the constant

term as time-independent, this uncorrelated part can be removed from the total signal to get the correlated part alone, as described in the paper of Kitamura et al. (2006). Fig. 10 shows the Rossi- α histogram for the 1061-configuration in EC5T from 0 to 100 ms. As can be seen, the first peak in the histogram is larger than the following ones due to the correlated part. After 80 ms, the correlated part is assumed to be negligible and the U-formed shape from 80 to 93 ms (13 ms source period) is subtracted from each period. The resulting exponential correlated part is depicted in Fig. 11. This procedure has been applied to most of the pulsed measurements of the two configurations. As for the slope fitting method, some data points in the beginning of each Rossi- α histogram had to be omitted in the function fitting procedure in order to achieve a satisfactory reduced χ^2 value.

As can be seen in Table 2, the results from the pulsed Rossi- α analysis are in good agreement with the slope fitting results. It should be mentioned that the uncertainties in the pulsed Rossi- α results are much larger than for the corresponding slope fitting results, although the measurement time was the same. This comes from the much more complicated data analysis that must be performed when utilising the pulsed Rossi- α method in comparison to the slope fitting. However, the accuracy of the pulsed Rossi- α method is better than for the traditional Rossi- α method (with a constant source) for similar measurement time. This comes from

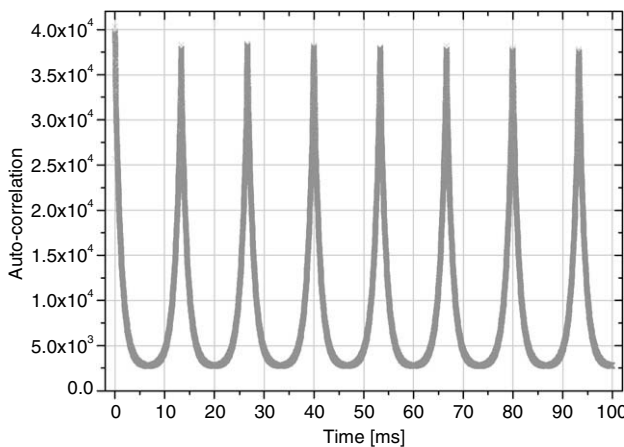


Fig. 10. Rossi- α histogram for the 1061-configuration in EC5T with pulsed neutron source.

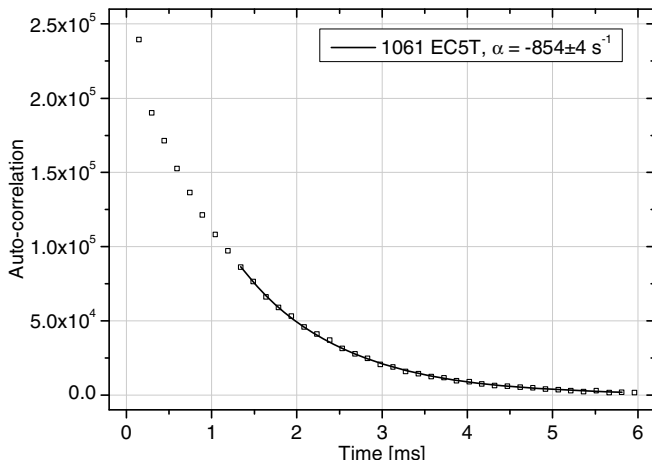


Fig. 11. The same Rossi- α histogram as in Fig. 10, but with the uncorrelated parts subtracted (and with different time discretization). The line indicates the fitted function.

Table 2
Results from pulsed Rossi- α measurements

Configuration	EC	α (s^{-1}) (slope fit.)	α (s^{-1}) (Rossi- α)
1132	EC5T	-654.1 ± 1.6	-671 ± 9
	EC8R	-648.7 ± 2.0	-618 ± 44
1061	EC5T	-875.0 ± 1.9	-854 ± 4
	EC6T	-892.1 ± 2.7	-881 ± 9
	EC7T	-866.7 ± 2.2	-890 ± 11
	EC8R	-863.4 ± 3.2	-868 ± 11
	EC9R	-860.1 ± 3.6	-842 ± 36

Table 3
Effective multiplication factor and effective delayed neutron fraction in pcm for the two configurations based on two nuclear data libraries

Configuration	JEFF3.1	JENDL3.3
1132	k_{eff}	0.97602 ± 0.00004
	β_{eff}	734.6 ± 6.5
1061	k_{eff}	0.96267 ± 0.00005
	β_{eff}	728.2 ± 8.9

the fact that the amplitude of the correlated term is much higher in the pulsed experiment, thus increasing the signal-to-noise ratio, but also due to the often higher count rate achievable with a pulsed source than for a ^{252}Cf -source (or other decay-based neutron source).

When comparing this pulsed Rossi- α study to that of Kitamura et al. (2006), one can notice that in this study the total correlation function for small t is almost as large as the uncorrelated part. This may cause problems when the uncorrelated part is subtracted. However, this study shows that the small difference is enough for the recovery of the prompt neutron decay constant with satisfactory accuracy.

6. Monte Carlo analysis

The Monte Carlo code MCNP (X-5 Monte Carlo Team, 2007) was used to analyse the experiment. An input deck was prepared, describing the conditions of the facility during the measurements on a very detailed level. During the preparation of the input deck it was found that traces of various isotopes in the construction materials (stainless steel, lead and cladding) could have large influence on the calculation results. After receiving results from chemical analysis of these materials, a proper material definition was created (Kiyavitskaya et al., 2007). The reliability of the input deck was ensured through comparisons based on various flux measurements at various locations in the core.

Based on the nuclear data libraries JEFF3.1 and JENDL3.3 (OECD/NEA, 2007) the effective multiplication factor for the two configurations was calculated. As can be seen in Table 3 both libraries suggest values around 0.976 and 0.963 for the two configurations respectively. The difference between the two libraries is only a few tens of pcm in both cases.

The effective delayed neutron fraction, β_{eff} , has been estimated based on the so called prompt method

$$\beta_{\text{eff}} = 1 - \frac{k_p}{k_{\text{eff}}} . \quad (14)$$

In this equation, k_p is the multiplication factor when transporting prompt neutrons only and k_{eff} is the effective multiplication factor with all neutrons included. Calculations were performed relying on the nuclear data libraries JEFF3.1 and JENDL3.3 and the results are shown in Table 3. No difference in effective delayed neutron fraction between the two configurations could be found. In the

following analysis, the value 733 ± 21 pcm will be used for both configurations representing both libraries. This value has been confirmed (Hogenbirk, 2007) based on the more exact method developed by Klein Meulekamp and van der Marck (2006). In this context, one must keep in mind that the definition of the integral kinetic parameters for source-driven systems is ambiguous (Dulla et al., 2006); however, the classical definitions (Keepin, 1965) will here be considered as sufficient.

7. Estimation of kinetic parameters

7.1. Effective multiplication factor

Knowing the reactivity in units of dollar and the effective delayed neutron fraction from MCNP, an experimental estimation of the effective multiplication constant can be obtained. By using the relation

$$k_{\text{eff}} = \frac{1}{1 - \left[\frac{\rho}{\beta_{\text{eff}}} \right]^{\text{exp}} \beta_{\text{eff}}^{\text{MCNP}}} \quad (15)$$

and the spread of ρ/β_{eff} as its uncertainty the result is $k_{\text{eff}} = 0.9747 \pm 0.0018$ for the 1132-configuration and $k_{\text{eff}} = 0.9650 \pm 0.0020$ for the 1061-configuration. The index "exp" means experimental value and "MCNP" means calculated value. When comparing these values with those obtained by MCNP one notices that the MCNP values are within the uncertainty of the inferred k_{eff} values above.

7.2. Neutron reproduction time

In the same way as for k_{eff} , an experimental estimation of the neutron reproduction time can be obtained based on Eq. (3) with the knowledge of β_{eff}

$$\Lambda = \frac{1}{\alpha^{\text{exp}}} \left(\left[\frac{\rho}{\beta_{\text{eff}}} \right]^{\text{exp}} - 1 \right) \beta_{\text{eff}}^{\text{MCNP}}. \quad (16)$$

The result is $\Lambda = 51.0 \pm 3.4 \mu\text{s}$ for the 1132-configuration and $\Lambda = 50.0 \pm 3.1 \mu\text{s}$ for the 1061-configuration. These values are typical for a thermal core rather than a fast core, indicating that the neutron multiplication process is mainly governed by the thermal part of the core. In fact, MCNP analysis of the booster zone alone with no fuel pins in the thermal zone shows that k_{eff} is as low as 0.6 for the fast zone, also indicating that a major part of the fissions required to maintain the fission chain reactions take place in the thermal zone.

The definition of the neutron reproduction time is ambiguous in a coupled fast-thermal core like YALINA-Booster, where there is a fast zone with kinetics different from the thermal zone. The neutron reproduction time discussed here represents a core averaged quantity.

8. Conclusions

Two subcritical configurations of the coupled fast-thermal core YALINA-Booster have been characterised based on pulsed neutron source measurements.

The slope fitting method showed good stability: less than 2% spread for all experimental channels. This is an indication that the point kinetic approximation, suggesting a single slope for the entire core, works well in the thermal part of the core.

The area ratio method suffers from a pronounced systematic spatial spread, however, the method was shown to be more stable than the extrapolated area ratio method. The extrapolated method tends to underestimate the multiplication factor far from the source and thereby underestimating the margin to criticality, which might be a safety concern. It was shown that the spatial

spread of the traditional area ratio method was not larger than making it possible to obtain the reactivity with an uncertainty of 200 pcm taking into account the uncertainty in the effective delayed neutron fraction as obtained from Monte Carlo simulations. It is worth noting that the conclusion that the slope fitting method is more stable than the area ratio method is in contrast to other experiments where the opposite condition has been reported (Jammes et al., 2005).

Prompt neutron decay constants obtained from the pulsed Rossi- α formula are in good agreement with those from the slope fitting method. However, it is much simpler to directly find the prompt neutron decay constant from the PNS histogram than performing the Rossi- α analysis. Thus, the pulsed Rossi- α method is less attractive for reactivity determination of pulsed systems.

It must be stressed that the only direct measurements have been performed on α and ρ/β_{eff} . The values of k_{eff} and Λ obtained from Eqs. (15) and (16) are only inferred values, based on the assumption that the simulated β_{eff} is correct within the uncertainty. Moreover, the result relies on the validity of the point-kinetics approximation. In this study, this validity was not investigated, as was done in the paper of Persson et al. (2005), since the very clear response function of the neutron pulse insertion did not raise such concerns.

Finally it is concluded that the neutron reproduction time of the YALINA-Booster core is comparable to that of a thermal system rather than a fast system.

Acknowledgements

The construction of the YALINA-Booster facility has been done within the framework of the Belarus State Scientific Program "Instruments for Scientific Research". The work performed at KTH was financially supported by Svensk Kärnbränslehantering AB, SKB (the Swedish Nuclear Fuel and Waste Management Co.). Financial support from the Swedish Institute making it possible to create scientific relation between Belarus and Sweden is cordially acknowledged.

References

- Bell, G.I., Glasstone, S., 1970. Nuclear Reactor Theory. Van Nostrand Reinhold Company.
- Dulla, S., Ravetto, P., Carta, M., d'Angelo, A., 2006. Kinetic parameters for source driven systems. In: International Conference on Advances in Nuclear Analysis and Simulation, PHYSOR 2006. Vancouver.
- Gozani, T., 1962. A modified procedure for the evaluation of pulsed source experiments in subcritical reactors. Nukleonik 4, 348.
- Hogenbirk, A., February 2007. NRG, Petten, Private communications.
- James, F., Winkler, M., 2004. MINUIT User's Guide. CERN, Geneva.
- Jammes, C., Geslot, B., Rosa, R., Imel, G., Fougeras, P., 2005. Comparison of reactivity estimations obtained from rod-drop and pulsed neutron source experiments. Annals of Nuclear Energy 32, 1131–1145.
- Kiyavitskaya, H., Bournos, V., Fokov, Y., Martsynkevich, B., Routkovskaya, C., Gohar, Y., Persson, C.-M., Gudowski, W., 2007. YALINA-Booster Benchmark Specifications for the IAEA Coordinated Research Projects on Analytical and Experimental Benchmark Analysis on Accelerator Driven Systems and Low Enriched Uranium Fuel Utilization in Accelerator Driven Sub-Critical Assembly Systems, IAEA.
- Kitamura, Y., Taguchi, K., Misawa, T., Pászit, I., Yamamoto, A., Yamanem, Y., Ichihara, C., Nakamura, H., Oigawa, H., 2006. Calculation of the stochastic pulsed Rossi-alpha formula and its experimental verification. Progress in Nuclear Energy 48, 37–50.
- Keepin, G.R., 1965. Physics of Nuclear Kinetics. Addison Wesley Publishing Company Inc., USA.
- Klein Meulekamp, R., van der Marck, S.C., 2006. Calculating the effective delayed neutron fraction with Monte Carlo. Nuclear Science and Engineering 152, 142–148.
- Lewis, J., 2006. Renaming the generation time the reproduction time. Annals of Nuclear Energy 33, 1071.
- Mellier, F. (coordinator) et al., 2005. The MUSE Experiments for Sub Critical Neutronics Validation, Deliverable No. 8, Final Report.
- OECD/NEA, 2002. Accelerator-driven Systems (ADS) and Fast Reactors (FR) in Advanced Nuclear Fuel Cycles – A Comparative Study.
- OECD/NEA, 2007. www.nea.fr.

- Persson, C.-M., Seltborg, P., Åhlander, A., Gudowski, W., Stummer, T., Kiyavitskaya, H., Bournos, V., Fokov, Y., Serafimovich, I., Chigrinov, S., 2005. Analysis of reactivity determination methods in the subcritical experiment Yalina. Nuclear Instruments and Methods in Physics Research A 554, 374–383.
- Rubbia, C., Monti, S., Salvatores, M., d'Angelo, A., Bignan, G., Burgio, N., Cacuci, D., Cahalan, J., Carta, M., Fougeras, P., Grangé, G., Imel, G., Jammes, C., Kadi, Y., Knebel, J., Maloy, S., Naberejnev, D.G., Philibert, H., Ravetto, P., 2003. TRADE: a full experimental validation of the ADS concept in a European perspective. In: AccApp'03, June 1–5, 2003, San Diego, California, USA.
- Simmons, B.E., King, J.S., 1958. A pulsed technique for reactivity determination. Nuclear Science and Engineering 3, 595–608.
- Sjöstrand, N.G., 1956. Measurement on a subcritical reactor using a pulsed neutron source. Arkiv för fysik 11, 13.
- Soule, R., Assal, W., Chaussonet, P., Destouches, C., Domergue, C., Jammes, C., Laurens, J.-M., Lebrat, J.-F., Mellier, F., Perret, G., Rimpault, G., Servière, H., Imel, G., Thomas, G.M., Villamarin, D., Gonzalez-Romero, E., Plaschy, M., Chawla, R., Kloosterman, J.L., Rugama, Y., Billebaud, A., Brissot, R., Heuer, D., Kerveno, M., Le Brun, C., Liatard, E., Loiseaux, J.-M., Méplan, O., Merle, E., Perdu, F., Vollaire, J., Baeten, P., 2004. Neutronic studies in support of accelerator-driven systems: the MUSE experiments in the MASURCA facility. Nuclear Science and Engineering 148, 124–152.
- X-5 Monte Carlo Team, 2007. MCNP – A General Monte Carlo N-Particle Transport Code, Version 5, LA-UR-03-1987.